Kinetics of the Gas-Phase Reaction of OH with HCl

Mikhail G. Bryukov and Barry Dellinger*

Department of Chemistry, Louisiana State University, Baton Rouge, Louisiana 70803

Vadim D. Knyazev

Research Center for Chemical Kinetics, Department of Chemistry, The Catholic University of America, Washington, D.C. 20064

Received: July 1, 2005; In Final Form: October 11, 2005

The reaction of hydroxyl radicals with hydrogen chloride (reaction 1) has been studied experimentally using a pulsed-laser photolysis/pulsed-laser-induced fluorescence technique over a wide range of temperatures, 298−1015 K, and at pressures between 5.33 and 26.48 kPa. The bimolecular rate coefficient data set obtained for reaction 1 demonstrates no dependence on pressure and exhibits positive temperature dependence that can be represented with modified three-parameter Arrhenius expression within the experimental temperature range: $k_1 = 3.20 \times 10^{-15} T^{0.99} \exp(-62\ \mathrm{K}/T)$ cm^3 molecule^{-1} s^{-1}. The potential-energy surface has been studied using quantum chemical methods, and a transition-state theory model has been developed for the reaction 1 on the basis of calculations and experimental data. The model results in modified three-parameter Arrhenius expressions: $k_1 = 8.81 \times 10^{-16} T^{1.16} \exp(58\ \mathrm{K}/T)$ cm^3 molecule^{-1} s^{-1} for the temperature range 200−1015 K and $k_1 = 6.84 \times 10^{-19} T^{2.12} \exp(646\ \mathrm{K}/T)$ cm^3 molecule^{-1} s^{-1} for the temperature dependence of the reaction 1 rate coefficient extrapolation to high temperatures (500−3000 K). A temperature dependence of the rate coefficient of the Cl + H_2O → HCl + OH reaction has been derived on the basis of the experimental data, modeling, and thermochemical information.

I. Introduction

Each year large quantities of toxic wastes containing chlorinated hydrocarbons (CHCs) are generated by chemical and allied industries. These materials are often disposed of in controlled, high-temperature incinerators, flared in an open flame, or subject to burning in uncontrolled fires as a result of transportation mishaps and other accidents. To assess and mitigate risks, it is necessary to understand and sometimes model all aspects of the combustion process. The understanding of the combustion chemistry is especially important in the case of CHCs, whose burning has the potential to generate toxic byproducts that are more hazardous than the original material. The presence of chlorine in the combustion or thermal degradation of organic compounds leads to the formation of different types of environmental pollutants such as phosgene, molecular chlorine, polychlorinated dibenzo-*p*-dioxins, polychlorinated dibenzofurans, and polychlorinated biphenyls.[1−3] Numerical simulation of the complicated chemistry of CHCs incineration requires a large database of accurately determined reaction rate coefficients spanning a wide range of temperatures and pressures. In this work, we report the results of our experimental and computational study of the gas-phase reaction of the hydroxyl radical with hydrogen chloride

$$\mathrm{OH} + \mathrm{HCl} \rightarrow \mathrm{H_2O} + \mathrm{Cl} \qquad (1)$$

over a wide temperature range.

HCl is one of the principal inorganic chlorine-containing species in combustion or thermal degradation of chlorinated organics; thus reaction 1 plays a significant role in the chemistry of these processes. In the early post-flame zone, it competes directly with the reaction of OH + CO, thus inhibiting CO oxidation.[2] Importantly, via reaction 1, HCl molecules are converted to Cl atoms, resulting in a potentially significant effect on the composition of the final emissions of chlorinated aromatic pollutants and molecular chlorine.[1−3] The importance of reaction 1 for atmospheric chemistry is described in various references.[4,5]

Reaction 1 has received ample attention from researches (refs 4−20), and most of these results are in an agreement at the low-temperature range (below ∼500 K). However, the only two direct measurements of the rate coefficient for this reaction conducted above ∼500 K (Ravishankara et al.,[4] 240−1055 K; Husain et al.,[14] 300−700 K) yields rate coefficient values that differ from each other by approximately a factor of 1.3 at 500 K and 1.7 at 700 K. This discrepancy indicates the need for additional measurements of the rate coefficient for reaction 1 at high temperatures. The current experimental study of the kinetics of reaction 1 has been performed in wide temperature range from 298 K (to compare with the earlier low-temperature studies) to 1015 K, which is relevant to combustion and thermal processes.

II. Experimental Section

Rate coefficient measurements were conducted in a heatable quartz reactor under pseudo-first-order conditions with a large excess of hydrogen chloride using the pulsed-laser photolysis (PLP) technique coupled with the pulsed-laser-induced fluorescence (PLIF) detection of the hydroxyl radicals. The experimental apparatus has been described in detail previously[21] and is considered here only briefly.

* To whom correspondence should be addressed. E-mail: BarryD@LSU.edu.

10.1021/jp053615x CCC: $33.50
Published on Web 12/14/2005

II.A. Experimental Apparatus. Our experimental approach utilized the PLP−PLIF technique combined with a heatable, slow-flow reactor to measure temporal profiles of relative OH concentrations. An excimer laser and an Nd:Yag-pumped, frequency-doubled, tunable pulsed dye laser were employed to generate the photolysis and probe laser pulses (beams), respectively.

The photolysis laser pulse was responsible for the creation of the hydroxyl radicals in the reactor. In most experiments, the hydroxyl radicals were formed following the 193-nm laser photolysis of nitrous oxide producing excited $O(^1D)$ atoms followed by rapid reaction with molecules of water[22,23]

$$N_2O + h\nu(193\ \text{nm}) \rightarrow N_2 + O(^1D) \quad (2)$$

$$O(^1D) + H_2O \rightarrow 2OH \quad (3)$$

When HCl was present in the reaction mixture, OH could potentially be produced via reaction of $O(^1D)$ with this species that can occur simultaneously with reaction 3. In selected experiments, we produced hydroxyl radicals by the 248-nm laser photolysis dissociation of HNO_3[5,24]

$$HNO_3 + h\nu(248\ \text{nm}) \rightarrow OH + NO_2 \quad (4)$$

to verify that the results were independent of the method of OH generation. At high reaction temperatures, to avoid possible effects from the thermal decomposition of N_2O and HNO_3 on the measurements of the rate coefficients, the hydroxyl radicals were formed by 193-nm laser dissociation of H_2O.[25]

After the pulse of the excimer laser, the pulse of the probe laser induced excitation of the hydroxyl radicals. OH was excited at approximately 282 nm via the $A^2\Sigma^+-X^2\Pi$ (1−0) transition followed by observation of fluorescence from the (1−1) and (0−0) bands at 308−316 nm (see, for example, refs 26 and 27). The fluorescent radiation emitted in a direction perpendicular to the plane defined by the two laser beams was monitored with a photomultiplier tube, using a UV band-pass filter (308 nm peak transmission) to minimize scattered light. The signal from the photomultiplier was amplified and then recorded by a 500-MHz digital oscilloscope to obtain the integrated voltage averaged for a desired number of laser pulses (typically 50−150) at single time delay. The value, S_t, received from the integration of the average voltage signal is a sum of two components: the integral from the average LIF signal of OH radicals, S_{OH} (this term is proportional to the absolute concentration of OH), and the integral from the average scattered light signal, S_{sc}. The average integrated voltage for the scattered light was measured directly in the absence of OH radicals. For this measurement, the photolysis laser was not triggered during the accumulation of the scattered light signal. Kinetic information was obtained by varying the time delay between pulses of the photolysis and the probe lasers in the desired time interval using a digital delay generator.

Helium was used as the main carrier gas in all experiments presented in this article. We utilized four separately controlled gas flows to prepare a reaction gas mixture. Three of them were the main flow of helium, the flow of nitrous oxide diluted with helium (100−1000 times) or the flow of helium containing nitric acid molecules, and the flow of helium containing water vapor. Nitric acid was added to the second flow of helium by bubbling helium through 70% nitric acid aqueous solution in thermostabilized saturator. Water vapor was added to the third flow of helium by bubbling helium through water at controlled pressure and temperature in another thermostabilized saturator. We employed three calibrated mass-flow controllers with appropriate flow ranges to establish the values of these three gas flows and maintain their stability throughout the duration of the experiments. At selected times during the experiments, we controlled values of these three flows by measuring rates of pressure increases in the calibrated volumes located upstream from the gas inlet of the reactor. These pressure measurements were performed with capacitance manometers of 100.00 and 1000.0 Torr ranges (1 Torr = 133.322 Pa).

The fourth flow was that of hydrogen chloride diluted with argon and was manually regulated with a metering valve. This flow was also determined by measuring the rate of the pressure increase in the calibrated volumes before and after obtaining each OH temporal profile. A mean value of these two flow measurements was taken to calculate HCl concentration in the reaction zone. The independence of the measured flows on the surface-to-volume ratio of the calibrated volume was verified to ensure the absence of interference from heterogeneous absorption and desorption processes on the walls of the volume. Hydrogen chloride was accurately, manometrically diluted with argon using Pyrex vacuum system and stored in a ∼22-L Pyrex bulb and a ∼9-L Pyrex cylindrical reservoir (∼13.5 cm inside diameter × ∼68 cm length). These two reservoirs with different surface-to-volume ratios were employed with the expressed purpose of verifying the absence of interference from heterogeneous absorption and desorption of HCl on the walls. To minimize systematic error in HCl concentration determination during all experiments, we had prepared seven HCl/Ar mixtures with different concentrations of HCl ranged between 4.59 and 17.10%, and these were used without any correlation between HCl concentrations in those and established reaction temperatures. All flows were premixed using a delivery system made of Pyrex, PFA, and Teflon and then directed through the pressure, temperature controlled, resistively heated quartz reactor. The composite flow conditioned the delivery system and the reactor for at least 15 min prior to data collection, thereby minimizing any effects due to reactant adsorption on the walls of the delivery system and the reactor, thus stabilizing the established experimental conditions. Pressure in the reactor was measured with the capacitance manometers described earlier. The maximum total uncertainty in the measurements of the reaction temperatures, T, did not exceed 0.5% of T. (See ref 21 for details.) The total flow rate ranged between 4.1 and 17.3 STP $cm^3\ s^{-1}$.

The molecular concentration of each reagent in the reaction zone was derived from its partial concentration, measurements of the flow rates, the reaction temperature, and total pressure under the ideal gas assumption. Typical reaction mixtures used in these experiments had concentrations in the ranges: N_2O, $8.0 \times 10^{13}-1.35 \times 10^{15}$ or 0.0; HNO_3, $1.0 \times 10^{14}-2.1 \times 10^{14}$ or 0.0; H_2O, $1.0 \times 10^{15}-3.0 \times 10^{15}$; He, $3.81 \times 10^{17}-3.25 \times 10^{18}$; Ar, $0.0-1.94 \times 10^{16}$; HCl , $0.0-2.71 \times 10^{15}$ in units of molecule cm^{-3}.

The chemicals utilized in this study had the following stated minimum purities (and were supplied by): He, 99.999% (The BOC Group, Inc.); Ar, 99.999% (The BOC Group, Inc.); HCl, 99.999% (Matheson Tri-Gas Inc.); N_2O, 9.98% mixture of 99.99% purity in 99.999% He (The BOC Group, Inc.); H_2O, A.C.S. reagent grade (Sigma-Aldrich); HNO_3 70% aqueous solution, A.C.S. reagent grade (Sigma-Aldrich). Analysis of HCl sample showed only trace levels of impurities, and these very small concentrations had negligible effect on the observed OH decay rates.

TABLE 1: Conditions and Results of Experiments to Measure Rate Coefficients of the Reaction of Hydroxyl Radicals with Hydrogen Chloride

no.[a]	T/K	P/kPa	[HCl] range/ 10^{14} molecule cm^{-3}	I^b/ mJ pulse^{-1} cm^{-2}	$[OH]_0$/ 10^{10} molecule cm^{-3}	$k_1{}^c$/ 10^{-13} molecule^{-1} cm^3 s^{-1}
1	298	13.37	3.15−22.5	5.5	15	7.38 ± 0.11
2	298	13.37	3.14−24.1	1.4	3.9	7.46 ± 0.39
3	321	6.66	1.43−26.5	0.50	8.8	8.03 ± 0.16
4	321	6.68	1.40−27.1	0.75	13	8.06 ± 0.17
5*	349	6.68	2.35−10.6	20	10	8.51 ± 0.31
6	403	13.38	2.22−11.1	4.7	17	10.46 ± 0.39
7	403	13.38	2.25−10.9	1.1	4	10.53 ± 0.64
8*	453	6.71	1.07−7.74	8.7	2.7	11.65 ± 0.62
9*	453	6.71	1.08−7.67	5.8	1.8	11.36 ± 0.47
10	517	13.37	1.19−10.5	3.8	28	13.40 ± 0.53
11	517	13.37	1.19−10.6	1.2	8.8	13.34 ± 0.33
12*	566	6.69	0.766−6.23	19	14	14.88 ± 0.58
13*	566	6.72	0.774−6.26	20	15	15.24 ± 0.42
14	650	13.39	0.81−8.59	0.19	1.4	17.90 ± 0.82
15	650	13.37	0.819−8.75	0.22	1.6	17.84 ± 0.37
16	650	13.40	0.782−8.69	0.95	7.0	18.10 ± 0.47
17	650	13.39	0.792−8.73	1.0	7.3	17.98 ± 0.38
18	700	13.34	0.617−11.4	0.85	7.8	19.71 ± 0.81
19	700	13.34	0.606−11.6	0.80	7.3	20.07 ± 0.78
20	756	6.73	0.689−5.02	0.65	39	21.78 ± 0.82
21	756	6.74	0.698−5.06	0.67	40	21.81 ± 0.92
22	820	13.35	0.589−5.77	7.3	20	22.9 ± 1.2
23	820	13.37	0.586−5.73	6.9	19	22.7 ± 1.2
24	820	13.36	0.582−5.81	1.8	5	23.51 ± 0.77
25$^+$	910	13.35	0.23−3.86	6.2	6.8	24.16 ± 0.91
26$^+$	910	26.48	0.618−4.14	2.6	5.1	24.8 ± 1.1
27$^+$	910	26.43	0.631−4.10	6.8	13	24.0 ± 1.3
28$^+$	1014	5.33	0.673−3.60	0.92	2.4	27.80 ± 0.84
29$^+$	1015	6.67	0.809−4.79	1.1	1.8	29.1 ± 1.9

[a] Experiment number. OH was produced by the PLP of HNO_3 at 248 nm in expepiments marked with an asterisk, OH was produced by the PLP of H_2O at 193 nm in experiments marked with a plus sign, and OH was formed by the 193-nm laser photolysis of N_2O to $O(^1D)$ and N_2 and the subsequent rapid reaction of $O(^1D)$ with H_2O in unmarked experiments. [b] Photolysis laser intensity. [c] Error limits represent 2σ statistical uncertainties only. Maximum estimated systematic uncertainty is 5% of the rate coefficient value (see text).

II.B. Reaction Rate Measurements and Data Processing. All experiments to measure the rate coefficients of reaction 1 were carried out under pseudo-first-order kinetic conditions with a large excess of hydrogen chloride [HCl] ≫ $[OH]_0$. An estimated initial concentration of OH radicals in the detection zone was in the range 1.4×10^{10}−4.0×10^{11} molecule cm^{-3}, at least 2 orders of magnitude smaller than the lowest HCl concentration in each set of experiments. Initial concentrations of OH radicals were estimated by a similar procedure described in ref 21 for experiments in which OH radicals were generated by the 193-nm pulsed laser photolysis of N_2O via processes 2 and 3 or by the 193-nm PLP of H_2O only. For experiments where OH was produced by the laser photolysis of HNO_3 at 248 nm, we estimated the initial concentrations of OH radicals in a manner similar to that performed in ref 24. The values of the initial concentrations of OH radicals used in the experiments to determine the rate coefficients of reaction 1 (listed in Table 1) are somewhat overestimated and should be understood as upper limits to $[OH]_0$. Nevertheless, the uncertainty in the ratio between any two values taken at the same temperature is ∼10%. Exact knowledge of the initial OH concentrations is not needed for determination of rate coefficients because the experiments were conducted under pseudo-first-order conditions with a large excess of hydrogen chloride. The evaluated detection sensitivity for OH radicals ranged from 1×10^8 to 3×10^8 molecule cm^{-3} depending on experimental conditions.

Examples of relative OH concentration temporal profiles of the set of experiments are presented in Figure 1 as a plot of $\ln(S_{OH})$ vs time delays, t. The initial detection time value, t_0, in all OH temporal decay profiles was not less than 0.28 ms. This time delay followed the photolysis of the reaction mixture and was sufficient for the completion of reaction 3 and/or for rotational and vibrational equilibration of OH radicals to the Boltzmann distribution.[23,28] In all experiments, water was added to reaction mixtures at a level of at least 1.0×10^{15} molecule cm^{-3} to ensure that these processes proceeded sufficiently fast (vide infra).

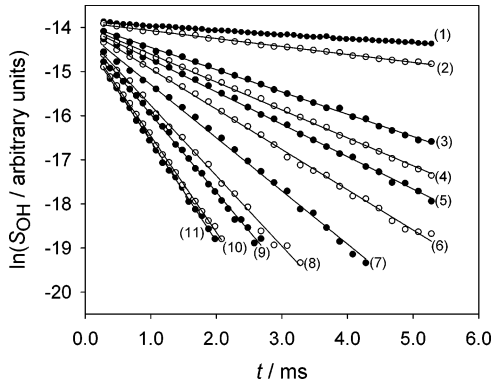

Figure 1. Examples of relative HO concentration temporal profiles obtained under the following conditions: helium buffer gas, temperature $T = 700$ K, total pressure $P = 13.34$ kPa (100.1 Torr), $[N_2O] = 2.94 \times 10^{14}$ molecule cm^{-3}, $[H_2O] = 1.2 \times 10^{15}$ molecule cm^{-3}; [HCl] = 0, 6.17×10^{13}, 2.32×10^{14}, 2.60×10^{14}, 3.04×10^{14}, 4.20×10^{14}, 5.26×10^{14}, 7.33×10^{14}, 8.18×10^{14}, 1.06×10^{15}, and 1.14×10^{15} molecule cm^{-3} for profiles 1−11, respectively.

We analyzed each set of the experiments at first assuming the first-order kinetic behavior of OH decay

$$\ln(S_{OH}) = \text{constant} - k't \qquad \text{(I)}$$

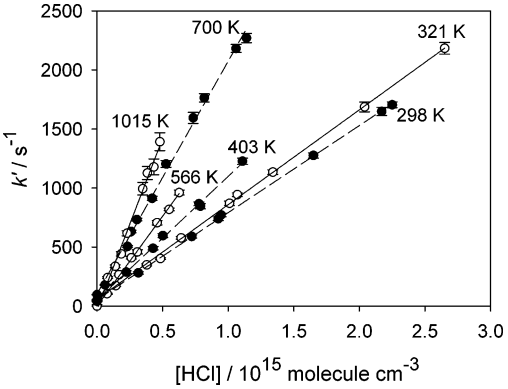

Figure 2. Examples of experimentally obtained k' vs [HCl] dependences.

where the effective first-order rate coefficient, k', is given by

$$k' = k_1[\mathrm{HCl}] + k_0 \qquad \text{(II)}$$

k_1 is the bimolecular rate coefficient for reaction 1, [HCl] is the hydrogen chloride concentration, and k_0 is the effective first-order rate coefficient of OH decay due to possible OH reactions with background impurities in the buffer gas, N_2O, H_2O, and HNO_3 precursors, OH reaction with HNO_3, and OH diffusion/flow out of the detection zone (OH background loss). The effective first-order rate coefficient values, k', were obtained from linear least-squares-fits of the experimental values $\ln(S_{OH})$ to eq I. (These least-squares fits and all other fits were performed with no weighting of the data points.) Examples of measured k' vs hydrogen chloride concentration dependencies are presented in Figure 2. We determined the bimolecular rate coefficient, k_1, from the slope of the least-squares straight line through the k' vs [HCl] data points including the (0, k_0) point, where k_0 was derived from OH temporal profile directly measured at zero concentration of HCl.

However, under some experimental conditions, the OH temporal profile detected at [HCl] = 0 and then plotted in (t, $\ln(S_{OH})$) coordinates displayed a reproducible positive curvature. It was experimentally found that the appearance of this curvature was mainly caused by the process of the OH diffusion out of the detection zone. All sets of the experiments with such behavior of OH background loss were also treated by data processing that is similar to that described in refs 29−32. In the first stage of these data processing, to obtain OH background-loss-corrected temporal profiles, each OH temporal profile of the set of the experiments recorded in the presence of HCl was point-by-point divided by the OH temporal profile recorded in the absence of hydrogen chloride. We extracted $k' = k_1[\mathrm{HCl}]$ (in this case) values from the OH background-loss-corrected temporal profiles using linear least-squares-fit procedure with two floating parameters and then determined the bimolecular rate coefficient, k_1, from the slope of the least-squares straight line (also with two floating parameters) through the ([HCl], k') data points including the (0, 0) point. For the same set of experiments, the application of data processing with the background loss correction stage always yielded a lower value for k_1 than the value obtained by applying the data processing without the background loss correction stage. Only in those cases where this difference was more than 1.0% of the k_1 value, the k_1 value obtained by the data processing with the background loss correction stage was taken as the result of its measurement for the subsequent consideration, instead of the k_1 value obtained assuming first-order kinetic behavior of OH decay. (See ref 21 and corresponding references therein for details.)

II.C. Experimental Results. Conditions and results of experiments to determine the values of the rate coefficients for reaction 1 are presented in Table 1. The kinetic study of the reaction of OH with HCl was performed over the wide temperature range of 298−1015 K and at pressures between 5.33 and 26.48 kPa. Over the entire experimental temperature range the initial concentration of the hydroxyl radicals was varied by changing the photolysis laser intensity and the concentrations of N_2O, HNO_3, and H_2O precursors in wide ranges from set to set of experiments. The measured rate coefficients demonstrate no correlation with reaction pressure or initial concentration of OH radicals within the experimental ranges. The observed pressure independence is anticipated, because the mechanism of the reaction is expected to be that of atom abstraction. The fact that the rate coefficients are independent of the initial OH radical concentrations indicates an absence of any influence of potential secondary reactions on the kinetics of OH radicals, as can be expected from the low values of $[\mathrm{OH}]_0$ (1.0×10^{10}−4.0×10^{11} molecule cm^{-3}) estimated as upper limits. Similarly, the observed absence of any correlation between the measured rate coefficients and the photolysis laser intensity and wavelength indicates that potential effects of reactions between OH and the products of the laser photolysis of HCl on the rate coefficient measurements are negligible. At the highest temperatures used in the study, the absence of any potential effects of thermal decomposition of hydrogen chloride was verified by measuring rate coefficients at different bulk flow velocities in the reactor varied by a factor of approximately 3.

In all experiments water was added to the reaction mixtures and its concentration was varied from 1.0×10^{15} to 3.0×10^{15} molecule cm^{-3} from set to set of experiments to ensure that the reaction 3[23] and/or rotational and vibrational equilibration of OH radicals to the Boltzmann distribution[28] proceeded sufficiently fast and had negligible effect on the measured rate coefficients. Moreover, over the entire experimental temperature range, we selectively detected temporal profiles of the formation of OH($\nu = 0$) under typical experimental conditions in the absence of hydrogen chloride. We observed a prompt OH($\nu = 0$) formation, which was always much faster than t_0. This indicates that reaction 3 and/or rotational and vibrational equilibration of OH radicals to the Boltzmann distribution proceeded fast enough to be neglected at the time delays $t \geq t_0$. Otherwise, a nonprompt OH($\nu = 0$) formation would be observed due to the lack of completion of these processes.

The values of the bimolecular rate coefficient for reaction 1, k_1, determined in this study with those from selected previous studies (vide infra) are presented on an Arrhenius plot in Figure 3. Our k_1 dataset exhibits positive temperature dependence with slight positive curvature in these coordinates, which can be reproduced by the modified three-parameter Arrhenius expression. A nonlinear least-squares fit of our k_1 experimental dataset yields the expression

$$k_1 = 3.20 \times 10^{-15} T^{0.99} \exp(-62\ \mathrm{K}/T)\ \mathrm{cm^3 molecule^{-1}\ s^{-1}}, \quad (298-1015\ \mathrm{K}) \qquad \text{(III)}$$

(Numbers in parentheses indicate the temperature range.) Maximum deviations of our experimental rate coefficient values from those calculated using the parametrized expression III is 5.6% of the calculated value. Error limits of the parameters in expressions III are not reported, because these parameters bear no physical meaning.

The error limits of the experimentally obtained rate coefficients listed in Table 1 represent the 2σ level of statistical

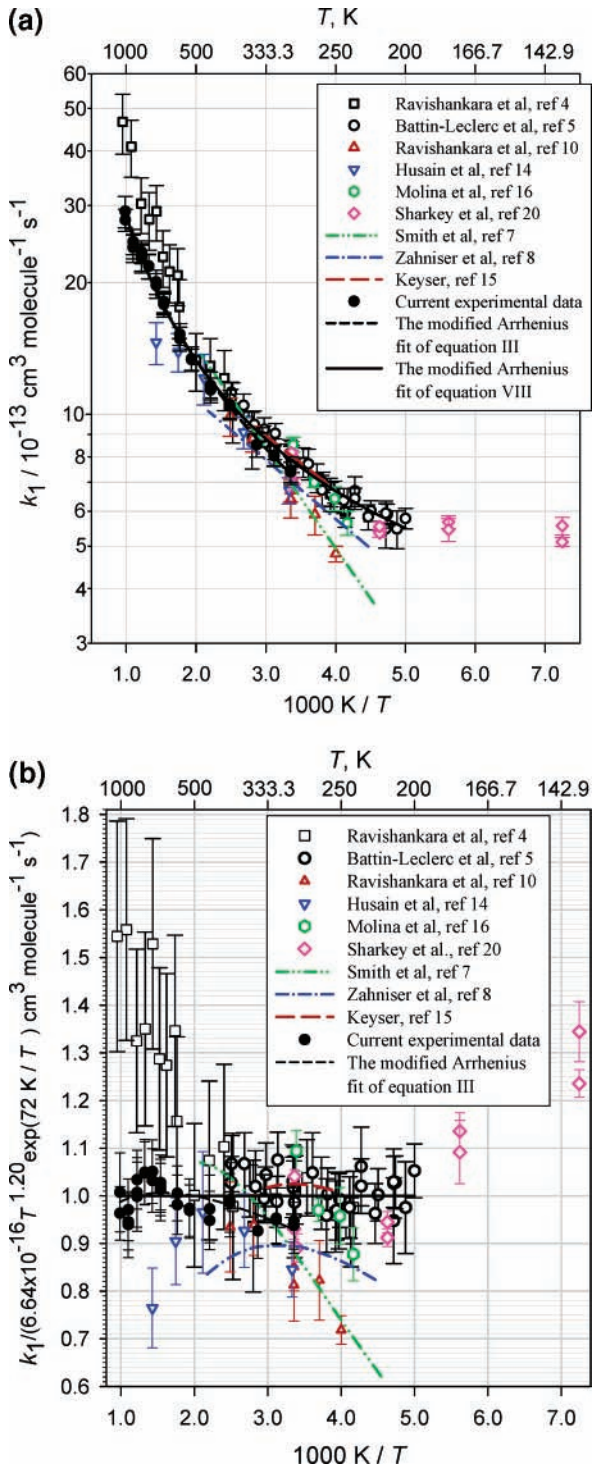

Figure 3. (a) Temperature dependence of the rate coefficient for the reaction of OH with HCl displayed in Arrhenius coordinates. Open black squares, black circles, red triangles up, blue triangles down, green hexagons, pink diamonds, and filled black circles represent experimental data from refs 4, 5, 10, 14, 16, 20, and current experimental data, respectively. Green dash−dot−dot, blue dash−dot, and red long dash lines represent temperature dependences recommended in refs 7, 8, and 15, respectively. Black short dash and solid line represent the modified Arrhenius fits of eqs III and VIII, respectively. (b) Rate coefficients for the reaction of OH with HCl normalized to a three-parameter fit of eq VIII. Open black squares, black circles, red triangles up, blue triangles down, green hexagons, pink diamonds, and filled black circles represent experimental data from refs 4, 5, 10, 14, 16, 20, and current experimental data, respectively. Green dash−dot−dot, blue dash−dot, and red long dash lines represent temperature dependences recommended in refs 7, 8, and 15, respectively. Black short dash represents the modified Arrhenius fit of eqs III.

(random) uncertainty only. The evaluated maximum of the systematic uncertainty in the experimental rate coefficients is 5% of the value. To determine the limits of these uncertainties, we subdivided the sources of error in the measured experimental physical parameters into statistical and systematic categories according to their physical nature or the behavior observed during the performance of the experiments.[21] The evaluation of potential systematic errors was mainly based on the finite accuracies stated by the manufacturers for the devices used in our experiments. The uncertainties in the measured experimental parameters were propagated to the final values of the uncertainties in the measured rate coefficients, using different mathematical procedures for propagating systematical and statistical uncertainties.[33]

III. Transition-State Theory Model of the OH + HCl Reaction

To provide means for an extrapolation of the experimental reaction 1 rate coefficient temperature dependence, $k_1(T)$, to temperatures outside the experimental range, a transition-state theory model of reaction 1 was created in the current work. In the initial approximation to the properties of the reaction transition state and geometry and vibrational frequencies obtained by Steckler et al.[34] and Battin-Leclerc et al.[5] in calculations performed at the CCSD(T)/cc-pVQZ//CCSD(T)/TZVP level were used, together with the experimental properties of the reactants and products.[54] The information within refs 34 and 5 was supplemented with additional quantum chemical calculations (using Gaussian 03[35]) to obtain the properties of the weakly bound OH···HCl complex and the values of barrier widths needed to evaluate tunneling contributions to the rate coefficients. Details of the barrier width-based approach to tunneling and the corresponding formalism can be found in refs 36−38.

The molecular structure, vibrational frequencies, and energy of the "entrance" OH···HCl complex (presented in the Supporting Information, Table 1S) were obtained in calculations performed at the same levels of quantum chemistry as was used in refs 34 and 5, i.e., CCSD(T)/TZVP for structure and frequencies and CCSD(T)/cc-pVQZ for single-point energy calculations.[39−44] The potential well depth of the complex was found to be 9.85 kJ mol^{-1} (including the vibrational zero-point energy, ZPE) relative to the reactants. The barrier width was obtained in fitting the intrinsic reaction coordinate maximum[45,46] energy profile obtained at the CCSD(T)/aug-cc-pVTZ//CCSD/TZVP level[43,44,47] (with ZPE obtained using projected vibrational frequencies[48,49] included) with the Eckart function.[50] In this potential-energy surface (PES) profile fitting, the reactant side energy asymptote of the Eckart function was matched with the energy of the "entrance" OH···HCl complex and that of the product side with the energy of the Cl + H_2O products. The value of the reaction energy barrier calculated at the CCSD(T)/aug-cc-pVTZ//CCSD/TZVP level (10.8 kJ mol^{-1}) agreed very well with that obtained in ref 5 at the higher CCSD(T)/cc-pVQZ//CCSD(T)/TZVP level (11.1 kJ mol^{-1}). Nevertheless, in rate coefficient calculations the energy barrier had to be lowered to match the experimental data (see below). When such adjustments were made, the barrier width was recalculated by scaling the electronic energy part of the PES profile (but keeping the ZPE contribution unchanged) to match the adjusted energy barrier and repeating the Eckart function fitting.

Rate coefficient values were calculated using the classical transition-state theory formula (see, for example, ref 51). Tunneling corrections $\kappa(T)$ were evaluated using the Eckart

formula[50] for the energy-dependent tunneling transition probability $P(E)$ and the equation[51]

$$\kappa(T) = \frac{1}{k_B T}\int_{E_{OH+HCl}}^{\infty} P(E)\exp\left(-\frac{E}{k_B T}\right) dE \qquad \text{(IV)}$$

Here, the energy of the reactants (OH + HCl) was taken as the lower integration limit. The transition state of reaction 1 has one torsional degree of freedom (internal rotation about the forming H−O bond). A relaxed PES scan of this internal rotation demonstrated that the structure of the −O−H−Cl atom sequence in the transition state varies from significantly nonlinear to almost linear with the change of the torsional angle and, at the same time, the reduced moment of inertia undergoes significant changes. These significant variations in the reduced moment of inertia indicate that treating this torsional degree of freedom as a one-dimensional internal rotation will not be accurate and therefore will not provide considerable advantages over treating it as a harmonic oscillator. Thus, a vibrator model was used for the transition state in all rate coefficient calculations. The presence in the transition state of two optical isomers differing by the values of the torsional angle resulted in the reaction path degeneracy of two.[52,53]

The properties of the reaction transition state obtained in quantum chemical calculations (refs 5 and 34), when used within the framework of the transition state theory cannot reproduce the experimental temperature dependence of the rate coefficient of reaction 1 (see below, in the Discussion section). The quantum chemistry based value of the reaction energy barrier, 11.1 kJ mol^{-1} with ZPE included, results in the slope of the Arrhenius graph at $T > 700$ K that is significantly larger than the experimental one. Thus, the value of the energy barrier required adjustment. Similarly, properties of the transition state that determine the pre-exponential factor also required modifications to match the experimental data. In particular, frequencies of the bending modes of the Cl−H−OH transitional structure are especially susceptible to error due to their coupling to the energy barrier.[56] Thus, to reproduce the experimental temperature dependence of the rate coefficient, an adjustment of the two lowest vibrational frequencies of the bending modes of the transition state and of the reaction barrier height were performed. A combined set of data formed by the results of the current study and those of Battin-Leclerc et al.[5] ($200 \le T \le 400$ K, included to represent the low-temperature $k_1(T)$ dependence) was used in the fitting (vide infra). The resultant model reproduces the experimental $k_1(T)$ dependence very well (Figure 4). The final adjusted value of the reaction energy barrier is 5.6 kJ mol^{-1}; the adjustment factor applied to the two lowest vibrational frequencies is 1.58 (the frequencies are increased); the value of the barrier width is 2.59 amu$^{1/2}$ Å.

The rate coefficient values calculated via modeling can be represented by the modified Arrhenius expressions

$$k_1 = 8.81\times10^{-16}T^{1.16}\exp(58\text{ K}/T)\text{ cm}^3\text{ molecule}^{-1}\text{ s}^{-1} \quad (200-1015\text{ K}) \quad \text{(V)}$$

$$k_1 = 6.84\times10^{-19}T^{2.12}\exp(646\text{ K}/T)\text{ cm}^3\text{ molecule}^{-1}\text{ s}^{-1} \quad (500-3000\text{ K}) \quad \text{(VI)}$$

providing good fits to the data in their respective temperature intervals with deviations from the computational values of less than 6 and 1%, respectively.

Information on reaction 1 obtained in the current work can be used in combination with the known thermochemistry ($\Delta H^0_{298} = -65.8$ kJ mol^{-1}, $\Delta S^0_{298} = -16.6$ J mol^{-1} K^{-1})[54,55] to derive the temperature dependence of the rate coefficient of the reverse process, that of the reactions of abstraction of a hydrogen atom from water by Cl

$$Cl + H_2O \rightarrow HCl + OH \quad (-1)$$

The transition-state theory model of reaction 1 created in the current study results in the $k_{-1}(T)$ dependence that can be represented by the expression

$$k_{-1} = 1.94\times10^{-16}T^{1.67}\times \exp(-7679\text{ K}/T)\text{ cm}^3\text{ molecule}^{-1}\text{ s}^{-1} \quad (200-3000\text{ K}) \quad \text{(VII)}$$

with deviations from the calculated values of less than 8%.

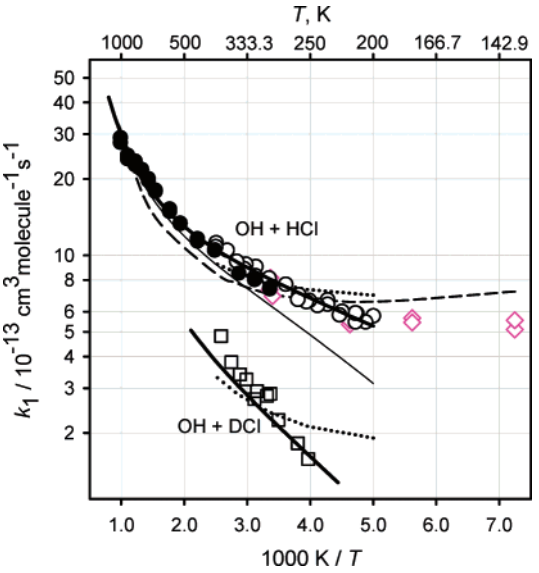

Figure 4. Selected experimental and calculated temperature dependences of the rate coefficients of the OH + HCl and OH + DCl reactions. Symbols: experimental values of the current study (filled black circles), ref 20 (open pink diamonds), and ref 5 (open black circles and squares). Lines: reaction models of the current study (heavy solid lines), ref 34 (dashed line), and ref 5 (dotted lines). To illustrate the contribution of tunneling, the values of k_1 calculated using the model of the current study with tunneling excluded are given by the thin solid line.

IV. Comparison with Previous Studies and Discussion

Reaction 1 plays an important role in the chemistry of atmospheric processes because HCl is a principal reservoir of inorganic chlorine (see, for example, refs 4 and 5); for this reason, the reaction has been extensively studied at low temperatures. To our knowledge, there have been 17 direct studies[4−20] of the kinetics of reaction 1. In refs 6, 12, 13, and 17−19, the rate coefficient for reaction 1 has been measured at room temperature only. In ref 9 the k_1 value at room temperature was reported and the temperature dependence of k_1 in the temperature range 293−567 K was found to be small. Ravishankara et al.[11] measured values of k_1 at 298 and 416 K, and obtained 7.0×10^{-13} and 1.16×10^{-12} cm^3 molecule^{-1} s^{-1}, respectively. All reported data in refs 6, 9, 11−13, 17−19 are in agreement with our data within combined experimental errors. These data are not plotted in Figure 3a to avoid congestion. In Figure 3a, we present the results of all previous direct studies[4,5,7,8,10,14−16,20] of the temperature-dependent kinetics of the reaction of OH + HCl.

The data set from ref 5 was included to represent the low-temperature $k_1(T)$ dependence for the purposes of rate coefficient

modeling, because it is the most extensive and recently obtained set of data for low temperatures. They are in good agreement and combine well with the current experimental $k_1(T)$ data set. Indeed, the least-squares fit of this combined dataset to the modified three-parameter Arrhenius expression gives

$$k_1 = 6.64 \times 10^{-16} T^{1.20} \exp(72\ \mathrm{K}/T)\ \mathrm{cm}^3\ \mathrm{molecule}^{-1}\ \mathrm{s}^{-1} \quad (200-1015\ \mathrm{K}) \quad \text{(VIII)}$$

with a relatively small maximum and average square deviation of 7.5 and 3.8%, respectively, between the combined experimental rate coefficient values and the rate coefficient values calculated using parametrized expression VIII.

In Figure 3b rate coefficients for the reaction of OH with HCl, normalized to a three-parameter fit of equation VIII, are plotted in order to show the comparison of the data more clearly. As can be seen from this figure low-temperature (below approximately 500 K) data and dependences obtained in studies 4, 8, 14−16, and 20 are in general agreement with our results combined with results from ref 5 within the reported experimental uncertainties in common temperature intervals. With concern of the data obtained by Ravishankara et al.[10] and temperature dependence recommended by Smith et al.,[7] these values are smaller than those calculated using expression VIII by factors of 1.4 and 1.6 at the lowest temperatures of these studies, 250 and 220 K, respectively. However, these data[7,10] are in agreement with our experimental data at room temperature and higher (see parts a and b of Figure 3).

Although reaction 1 is important for the understanding of the combustion and thermal degradation chemistry of CHCs, there have only been two previous studies[4,14] that extend to high temperatures (above approximately 500 K) and are relevant to combustion and thermal processes. Our experimental data set of k_1 values generally lies between those obtained in refs 4 and 14. The experimental data from ref 14 are systematically lower than k_1 values calculated using eq VIII. From 300 to 573 K, they are in agreement with eq VIII within experimental errors, but at the highest temperature of the study,[14] 700 K, the obtained k_1 value is lower by 24% than that calculated using eq VIII. The experimental data from ref 4 are also in agreement with eq VIII in the range 240−568 K within experimental errors. Above 568 K these data lie higher than values given by expression VIII by at least 27%, and the deviation reached a maximum of 56% at the highest common temperature.

Ravishankara et al.[4] pointed out that the probable reason for the lower measured k_1 values is overestimation of the HCl concentration due to the loss of HCl on the walls of the delivery system and/or the reactor under static and even under slow flow conditions. The authors of the work[10] observed a decrease in rate coefficient with increased residence time in their static system, which could be explained by this effect. The HCl wall loss problem is likely to increase with decreasing temperature, and it may be significant in low temperature studies. Nevertheless, to verify the absence of interference from HCl heterogeneous absorption and desorption processes on the walls of the vacuum and delivery systems, and the reactor, in our experiments we varied the following parameters: the surface-to-volume ratio of the calibrated Pyrex vessels used to measure the flows (varied by a factor of approximately 3) and Pyrex vessels for HCl/Ar mixture preparation and storage; the HCl concentration of the HCl/Ar mixtures (see subsection II.A. of the present article); bulk flow velocity in the delivery system and in the reactor varied by a factor of approximately 8 and 3, respectively; and pressure (see Table 1). No correlation was found between those parameters and the obtained rate coefficients. Invariance of the measured rate coefficients with respect to the parameters described here and in subsection II.C gives us confidence in the rate coefficients determined in the present work.

Reaction 1 was previously subjected to computational modeling, with the most advanced theoretical model of this reaction presented by Steckler at al.[34] and, with minor modifications, by Battin-Leclerc.[5] These authors used high-level quantum chemical calculations to evaluate the reaction PES (see above) and applied canonical variational transition state theory with multidimensional tunneling model based on semiclassical treatment to obtain the rate coefficient values. The resultant $k_1(T)$ dependences are presented in Figure 4 along with the experimental results of the current study and those of Battin-Leclerc[5] and Sharkey and Smith[20] as well as the calculated $k_1(T)$ dependence obtained in the current work. As one can see from the plot, one significant advantage of the model of refs 34 and 5 is that, qualitatively, it correctly describes the shape of the $k_1(T)$ dependence: the reaction rate is essentially temperature independent at low temperatures but increases with temperature at high temperatures. The degree of the quantitative agreement, however, does not allow use of this model for extrapolation of the rate coefficients outside the experimental temperature ranges. The calculated line of ref 34 crosses the experimental $k_1(T)$ dependence at two temperatures and displays a significantly larger curvature of the Arrhenius plot and larger high-temperature activation energy compared with those obtained in experiments.

The model of reaction 1 developed in the current study also has its limitations. In particular, the resultant calculated $k_1(T)$ dependence, if extrapolated to lower temperatures, will disagree with the experimental results of Sharkey and Smith in the 138−200 K range (Figure 4). This disagreement indicated that, most likely, the contribution of tunneling at low temperatures is underestimated. However, the primary objective of the current investigation of reaction 1 is elucidation of its kinetics at high temperatures relevant to combustion and other thermal processes. At these high temperatures, the uncertainty introduced by an imperfect description of tunneling can be expected to be minor. To estimate the effects of this tunneling uncertainty, the model-fitting exercise described in section III was repeated with two modified versions of the model, one with increased and another with decreased tunneling corrections. In both cases, tunneling corrections were modified by multiplying or dividing the barrier width by a factor of 1.5. The corresponding increase and decrease in the 200 K tunneling correction were 78% (increase) and 33% (decrease). The resultant changes in the high-temperature rate coefficients described by the fitted models differ from the central model by not more than 19% (increased tunneling) or not more than 10% (decreased tunneling). The model with the increased tunneling produced excessive curvature in the Arrhenius plot that was visibly larger than the experimental curvature.

To further evaluate the model performance, kinetic isotope effects were considered. Temperature dependences of the rate coefficients for the reactions of OH (and OD) with HCl and DCl were obtained by Battin-Leclerc et al.[5] in the approximately 200−400 K range. Substitution of H with D in the hydroxyl radical was demonstrated to have only a minor effect on the rate coefficient values, as can be expected since the hydrogen atom in OH does not directly participate in the reaction. At the same time, substitution of DCl for HCl results in a decrease of the rate coefficient by approximately a factor of 2−4, depending

on the temperature. The model for the OH + DCl reaction was created in the current work on the basis of the OH + HCl model by using the vibrational frequencies of Steckler et al.[34] and Battin-Leclerc et al.[5] for the transition state and applying the same 1.58 factor (see section III) to the two lowest bending frequencies, using experimental[54] properties of DCl, modifying the fitted OH + HCl energy barrier by the difference in the ZPE (+1.52 kJ mol^{-1}) and increasing the barrier width parameter by the square root of the D/H mass ratio (the resultant barrier width value is 3.66 $amu^{1/2}$ Å). The rate coefficient values obtained for the OH + DCl reaction demonstrate good agreement with the experimental data (Figure 4), which provides further support to the model of the OH + HCl reaction.

To summarize, we recommend expressions V or VIII for the temperature dependence of the reaction 1 rate coefficient in the temperature range from 200 to 1015 K. These two expressions give practically the same values of $k_1(T)$, because the maximum deviation between them is less than 0.8%. For the temperature dependence of the reaction 1 rate coefficient extrapolation, outside the experimental range to high temperatures up to 3000 K, we recommend expression VI.

Acknowledgment. This research was supported by the Patrick F. Taylor Chair Foundation. The authors would like to thank Mr. S. Bagley, Dr. J. Hogan, and Dr. V. L. Orkin for helpful discussion and advice.

Supporting Information Available: A supplement, including the results of the quantum chemical calculations on the OH···HCl complex (Table 1S, one page). This material is available free of charge via the Internet at http://pubs.acs.org.

References and Notes

(1) Chang, W.-D.; Senkan, S. M. *Environ. Sci. Technol.* **1989**, *23*, 442.

(2) Procaccini, C.; Bozzelli, J. W.; Longwell, J. P.; Smith, K. A.; Sarofim, A. F. *Environ. Sci. Technol.* **2000**, *34*, 4565.

(3) Procaccini, C.; Bozzelli, J. W.; Longwell, J. P.; Sarofim, A. F.; Smith, K. A. *Environ. Sci. Technol.* **2003**, *37*, 1684.

(4) Ravishankara, A. R.; Wine, P. H.; Well, J. R.; Thompson, R. L. *Int. J. Chem. Kinet.* **1985**, *17*, 1281.

(5) Battin-Leclerc, F.; Kim, I. K.; Talukdar, R. K.; Portmann, R. W.; Ravishankara, A. R. *J. Phys. Chem. A* **1999**, *103*, 3237.

(6) Takacs, G. A.; Glass, G. P. *J. Phys. Chem.* **1973**, *77*, 1948.

(7) Smith, I. W. M.; Zellner, R. *J. Chem. Soc., Faraday Trans. 2* **1974**, *70*, 1045.

(8) Zahniser, M. S.; Kaufman, F.; Anderson, J. G. *Chem. Phys. Lett.* **1974**, *27*, 507.

(9) Hack, W.; Mex, G.; Wagner, H. Gg. *Ber. Bunsen-Ges. Phys. Chem.* **1977**, *81*, 667.

(10) Ravishankara, A. R.; Smith, G.; Watson, R. T.; Davis, D. D. *J. Phys. Chem.* **1977**, *81*, 2220.

(11) Ravishankara, A. R.; Wine, P. H.; Langford, A. O. *Chem. Phys. Lett.* **1979**, *63*, 479.

(12) Husain, D.; Plane, J. M.; Slater, N. K. H. *J. Chem. Soc., Faraday Trans. 2* **1981**, *77*, 1949.

(13) Cannon, B. D.; Robertshaw, J. S.; Smith, I. W. M.; Williams, M. D. *Chem. Phys. Lett.* **1984**, *105*, 380.

(14) Husain, D.; Plane, J. M. C.; Xiang, C. C. *J. Chem. Soc., Faraday Trans. 2* **1984**, *80*, 713.

(15) Keyser, L. F. *J. Phys. Chem.* **1984**, *88*, 4750.

(16) Molina, M. J.; Molina, L. T.; Smith, C. A. *Int. J. Chem. Kinet.* **1984**, *16*, 1151.

(17) Smith, I. W. M.; Williams, M. D. *Ber. Bunsen-Ges. Phys. Chem.* **1985**, *89*, 319.

(18) Smith, I. W. M.; Williams, M. D. *J. Chem. Soc., Faraday Trans. 2* **1986**, *82*, 1043.

(19) Orkin, V. L.; Khamaganov, V. G.; Larin, I. K. *Int. J. Chem. Kinet.* **1993**, *25*, 67.

(20) Sharkey, P.; Smith, I. W. M. *J. Chem. Soc., Faraday Trans.* **1993**, *89*, 631.

(21) Bryukov, M. G.; Knyazev, V. D.; Lomnicki, S. M.; McFerrin, C. A.; Dellinger, B. *J. Phys. Chem. A* **2004**, *108*, 10464.

(22) Droege, A. T.; Tully, F. P. *J. Phys. Chem.* **1986**, *90*, 1949.

(23) Atkinson, R.; Baulch, D. L.; Cox, R. A.; Hampson, R. F., Jr.; Kerr, J. A.; Rossi, M. J.; Troe, J. *J. Phys. Chem. Ref. Data* **1997**, *26*, 1329.

(24) Gilles, M. K.; Burkholder, J. B.; Ravishankara, A. R. *Int. J. Chem. Kinet.* **1999**, *31*, 417.

(25) Dunlop, J. R.; Tully, F. P. *J. Phys. Chem*. **1993**, *97*, 11148.

(26) Wollenhaupt, M.; Carl, S. A.; Horowitz, A.; Crowley, J. N. *J. Phys. Chem. A* **2000**, *104*, 2695.

(27) D'Ottone, L.; Campuzano-Jost, P.; Bauer, D.; Hynes, A. J. *J. Phys. Chem. A* **2001**, *105*, 10538.

(28) Silvente, E.; Richter, A. C.; Hynes, A. J. *J. Chem. Soc., Faraday Trans.* **1997**, *93*, 2821.

(29) Tully, F. P.; Golgsmith, J. E. M. *Chem. Phys. Lett.* **1985**, *116*, 345.

(30) Tully, F. P.; Droege, A. T.; Koszykowski, M. L.; Melius, C. F. *J. Chem. Phys.* **1986**, *90*, 691.

(31) Orkin, V. L.; Huie, R. E.; Kurylo, M. J. *J. Phys. Chem.* **1996**, *100*, 8907.

(32) Kurylo, M. J.; Orkin, V. L. *Chem. Rev.* **2003**, *103*, 5049.

(33) Bevington, P. R. *Data Reduction and Error Analysis for the Physical Sciences*; McGraw-Hill: New York, 1969.

(34) Steckler, R.; Thurman, G. M.; Watts, J. D.; Bartlett, R. J. *J. Chem. Phys.* **1997**, *106*, 3926.

(35) Frisch, M. J.; Trucks, G. W.; Schlegel, H. B.; Scuseria, G. E.; Robb, M. A.; Cheeseman, J. R.; Montgomery, J. A., Jr.; Vreven, T.; Kudin, K. N.; Burant, J. C.; Millam, J. M.; Iyengar, S. S.; Tomasi, J.; Barone, V.; Mennucci, B.; Cossi, M.; Scalmani, G.; Rega, N.; Petersson, G. A.; Nakatsuji, H.; Hada, M.; Ehara, M.; Toyota, K.; Fukuda, R.; Hasegawa, J.; Ishida, M.; Nakajima, T.; Honda, Y.; Kitao, O.; Nakai, H.; Klene, M.; Li, X.; Knox, J. E.; Hratchian, H. P.; Cross, J. B.; Bakken, V.; Adamo, C.; Jaramillo, J.; Gomperts, R.; Stratmann, R. E.; Yazyev, O.; Austin, A. J.; Cammi, R.; Pomelli, C.; Ochterski, J. W.; Ayala, P. Y.; Morokuma, K.; Voth, G. A.; Salvador, P.; Dannenberg, J. J.; Zakrzewski, V. G.; Dapprich, S.; Daniels, A. D.; Strain, M. C.; Farkas, O.; Malick, D. K.; Rabuck, A. D.; Raghavachari, K.; Foresman, J. B.; Ortiz, J. V.; Cui, Q.; Baboul, A. G.; Clifford, S.; Cioslowski, J.; Stefanov, B. B.; Liu, G.; Liashenko, A.; Piskorz, P.; Komaromi, I.; Martin, R. L.; Fox, D. J.; Keith, T.; Al-Laham, M. A.; Peng, C. Y.; Nanayakkara, A.; Challacombe, M.; Gill, P. M. W.; Johnson, B.; Chen, W.; Wong, M. W.; Gonzalez, C.; Pople, J. A. *Gaussian 03*, revision C.02; Gaussian, Inc.: Wallingford, CT, 2004.

(36) Knyazev, V. D.; Bencsura, A.; Stoliarov, S. I.; Slagle, I. R. *J. Phys. Chem.* **1996**, *100*, 11346.

(37) Knyazev, V. D.; Slagle, I. R. *J. Phys. Chem*. **1996**, *100*, 16899.

(38) Bryukov, M. G.; Slagle, I. R.; Knyazev, V. D. *J. Phys. Chem. A* **2001**, *105*, 3107.

(39) Cizek, J. *Adv. Chem. Phys.* **1969**, *14*, 35.

(40) Purvis, G. D. I.; Bartlett, R. J. *J. Chem. Phys.* **1982**, *76*, 1910.

(41) Pople, J. A.; Head-Gordon, M.; Raghavachari, K. *J. Chem. Phys.* **1987**, *87*, 5968.

(42) Schaefer, A.; Horn, H.; Ahlrichs, R. *J. Chem. Phys.* **1994**, *100*, 5829.

(43) Dunning, T. H., Jr. *J. Chem. Phys.* **1989**, *90*, 1007.

(44) Woon, D. E.; Dunning, T. H., Jr. *J. Chem. Phys.* **1993**, *98*, 1358.

(45) Malick, D. K.; Petersson, G. A.; Montgomery, J. A. J. *J. Chem. Phys.* **1998**, *108*, 5704.

(46) Petersson, G. A.; Irikura, K. K.; Frurip, D. J. American Chemical Society: Washington, DC, 1998.

(47) Kendall, R. A.; Dunning, T. H., Jr.; Harrison, R. J. *J. Chem. Phys.* **1992**, *96*, 6796.

(48) Miller, H. W.; Handy, N. C.; Adams, J. E. *J. Chem. Phys.* **1980**, *72*, 99.

(49) Baboul, A. G.; Schlegel, H. B. *J. Chem. Phys.* **1997**, *107*, 9413.

(50) Eckart, C. *Phys. Rev.* **1930**, *35*, 1303.

(51) Johnston, H. S. *Gas-Phase Reaction Rate Theory*; The Ronald Press: New York, 1966.

(52) Pechukas, P. *Dynamics of Molecular Collisions*; Miller, W. H., Ed.; Plenum Press: New York, 1976; Vol. Part B.

(53) Karas, A. J.; Gilbert, R. G.; Collins, M. A. *Chem. Phys. Lett.* **1992**, *193*, 181.

(54) Chase, M. W., Jr. *J. Phys. Chem. Ref. Data* **1998**, *Monograph 9*, 1−1951.

(55) Ruscic, B.; Wagner, A. F.; Harding, L. B.; Asher, R. L.; Feller, D.; Dixon, D. A.; Peterson, K. A.; Song, Y.; Qian, X. M.; Ng, C. Y.; Liu, J. B.; Chen, W. W. *J. Phys. Chem. A* **2002**, *106*, 2727.

(56) Donahue, N. M. *J. Phys. Chem. A* **2001**, *105*, 1489.